

RESEARCH ARTICLE

A 1200+ year reconstruction of temperature extremes for the northeastern Mediterranean region

Lara Klippel¹  | Paul J. Krusic^{2,3,4} | Oliver Konter¹ | Scott St. George⁵ | Valerie Trouet⁶ | Jan Esper^{1,4}

¹Department of Geography, Johannes Gutenberg University, Mainz, Germany

²Department of Geography, University of Cambridge, Cambridge, UK

³Department of Physical Geography, Stockholm University, Stockholm, Sweden

⁴Navarino Environmental Observatory, Messinia, Greece

⁵Department of Geography, Environment and Society, University of Minnesota, Minneapolis, Minnesota

⁶Laboratory of Tree-Ring Research, University of Arizona, Tucson, Arizona

Correspondence

Lara Klippel, Department of Geography, Johannes Gutenberg University, 55099 Mainz, Germany.
Email: l.klippel@geo.uni-mainz.de

Funding information

Deutsche Forschungsgemeinschaft, Grant/Award Number: ES 161/9-1Inst 247/665-1 FUGG; National Science Foundation, Grant/Award Number: AGS-1349942

Proxy evidence is necessary to place current temperature and hydroclimatic changes in a long-term context and to assess the full range of natural and anthropogenic climate forcings. Here, we present the first millennium-length reconstruction of late summer (August–September) temperature variability for the Mediterranean region. We compiled 132 maximum latewood density (MXD) tree-ring series of living and relict *Pinus heldreichii* trees from a network of four high-elevation sites in the Pindus Mountains of Greece. Forty series reach back into the first millennium and the oldest sample dates to 575 CE. At annual to decadal scales, the record correlates significantly with August–September temperatures over the Balkan Peninsula and northeastern Mediterranean ($r_{1950-2014} = 0.71$, $p < 0.001$). We produce two reconstructions emphasizing interannual and decadal scale variance over the past millennium. Analysis of temperature extremes reveals the coldest summers occurred in 1035, 1117, 1217, 1884 and 1959 and the coldest decades were 1061–1070 and 1811–1820. The warmest summers occurred in 1240 and 1474, and the warmest decades were 1141–1150 and 1481–1490. Comparison of this new reconstruction with MXD-based summer temperature reconstructions across Europe reveals synchronized occurrences of extreme cool summers in the northeastern Mediterranean, and an antiphase-relationship with warm summer temperatures over the British Isles and Scandinavia. This temperature dipole is related to anomalies in the latitudinal position of the North Atlantic Jet. Despite the representation of common atmospheric forcing patterns, the occurrence of warm extremes is limited to few events, suggesting potential weaknesses of MXD to record warm temperature anomalies. In addition, we acknowledge problems in the observational data to capture local temperature variability due to small scale topographic differences in this high-elevation landscape. At a broader geographical scale, the occurrence of common cold summer extremes is restricted to years with volcanically induced changes in radiative forcing.

KEYWORDS

dendroclimatology, maximum latewood density, Mediterranean climate, North Atlantic Jet, *Pinus heldreichii*, temperature reconstruction

1 | INTRODUCTION

In the Mediterranean region, an overall warming trend (Xoplaki *et al.*, 2003a; Alexandrov *et al.*, 2004; Philandras *et al.*, 2008; Toreti *et al.*, 2009) has prevailed in the 20th

century, with increasing frequency of hot summer temperature extremes (Kostopoulou and Jones, 2005; Diffenbaugh *et al.*, 2007). The intensity, length, and number of heat waves along the western Balkans and southern Black Sea coast have risen since the 1960s (Kuglitsch *et al.*, 2010).

Climate models agree on a persistent summer temperature increase in coming decades (Li *et al.*, 2012), accompanied by extremely hot summers, which occurred only rarely during the past decades, but are projected to become common in the second half of the 21st century (Lelieveld *et al.*, 2013). Additionally, risks of summer drought extremes are increasing in west-central Mediterranean regions (Alpert, 2002; Sousa *et al.*, 2011; Hoerling *et al.*, 2012; Vicente-Serrano *et al.*, 2014; Spinoni *et al.*, 2015) affecting the overall fire risk (Moriondo *et al.*, 2006). Meteorological records reveal a precipitation decrease in the eastern Mediterranean (García-Herrera *et al.*, 2007) and extreme drought episodes have become more frequent and persistent (Xoplaki *et al.*, 2004). In a centennial-to-millennial scale context, proxy-based climate reconstructions are needed to evaluate current climatic trends and changes in the frequency and magnitude of extremes, and to assess the full range of projected forcing impacts (Ljungqvist *et al.*, 2016). Proxy archives also provide the background to study the impact of climate on societies and economies (Büntgen *et al.*, 2011; Xoplaki *et al.*, 2016) and support the differentiation between naturally and anthropogenically forced variations.

Tree growth at high-elevation sites in the Mediterranean region is typically influenced by a combination of temperature and precipitation (Seim *et al.*, 2012; Trouet *et al.*, 2012) limiting the use of tree-ring width (TRW) as a temperature proxy (Esper *et al.*, 2016). Multiple TRW records and reconstructions have been produced in the region with hydroclimate as the dominant climatic signal (Akkemik and Aras, 2005; Touchan *et al.*, 2005; Griggs *et al.*, 2007; Akkemik *et al.*, 2008; Köse *et al.*, 2011; Levanić *et al.*, 2012; Seim *et al.*, 2012; Esper *et al.*, 2014b; Klesse *et al.*, 2015; Tejedor *et al.*, 2016; Klippel *et al.*, 2017; Klippel *et al.*, 2018). Progress has also been made in the assessment of long-term temperature dynamics based on indices from documentary sources (Camuffo *et al.*, 2010; Kiss *et al.*, 2011). In dendroclimatology, maximum latewood density (MXD) from *P. heldreichii* (PIHE) in central–eastern Mediterranean tree-line forests was shown to contain a robust July–September temperature signal ($r > 0.6$; Trouet *et al.*, 2012; Klesse *et al.*, 2015). PIHE MXD derived temperature reconstructions have been developed for the Mt. Olympus region in Greece (1521–2010; Klesse *et al.*, 2015), the Pirin Mountains in Bulgaria (1768–2008; Trouet *et al.*, 2012), multiple sites in the northeastern Mediterranean basin (1675–1980; Trouet, 2014), and Italy (1650–1980; Leonelli *et al.*, 2017). However, millennium-length MXD chronologies have not yet been developed for the region, which limits our understanding of the occurrence, magnitude, and possible causes of naturally forced temperature extremes. Prior to 1550 CE (Klesse *et al.*, 2015), regional temperature information is available solely from low resolution (decadal to multi-decadal) proxy archives (Grauel *et al.*, 2013; Gogou *et al.*, 2016; Izdebski *et al.*, 2016).

Millennium-length MXD based temperature reconstructions have been produced in locations where tree growth is temperature limited and wood material has been preserved for several hundreds of years (Esper *et al.*, 2016). In Europe, MXD chronologies spanning the past millennium have been developed at the northern tree line in Scandinavia (Esper *et al.*, 2012; Melvin *et al.*, 2013; Linderholm *et al.*, 2014; Esper *et al.*, 2014a) and at the elevational tree line in the Pyrenees (Büntgen *et al.*, 2008; Dorado Liñán *et al.*, 2012; Büntgen *et al.*, 2017b) and Alps (Schweingruber *et al.*, 1988; Büntgen *et al.*, 2006). Especially in the Mediterranean region, an improved spatial distribution of high-resolution proxy archives is required to refine our knowledge about pre-instrumental climate variability patterns and their association with natural forcings at regional to continental scales (Pages 2k PMIP3 Group, 2015).

Here, we address these topics by (1) introducing a new MXD tree-ring chronology from 132 density profiles of living and relict high-elevation pine trees in the Pindus Mountains of Greece, that covers the period 738–2014 CE and reflects August–September temperature variability; (2) identifying past temperature extremes at annual-to-decadal scales, as well as detecting their spatial extent and association with atmospheric patterns and climatic forcings.

2 | DATA AND METHODS

2.1 | Geographical settings and sampling design

Between 2011 and 2016, 47 cores and 85 discs were collected at four *P. heldreichii* sites, with different exposures within the tree line ecotone at 2,100 m. a.s.l on Mt. Smolikas (SMO) (Figure 1a–c; subset of Klippel *et al.*, 2017). MXD measurements are produced using the high-precision DENDRO2003 X-ray radio densitometer from Walesch Electronic. Samples were prepared according to standard dendrochronological techniques for X-ray exposure (Lenz *et al.*, 1976; Schweingruber *et al.*, 1978). Cores and wedges are treated for 34 hr with alcohol in a Soxhlet to extract resins and other compounds. Each sample was split into 3 cm long sections to avoid biases from internal changes in stem-fibre direction. Two millimetre thick laths from these sections are cut perpendicular to the tracheid's longitudinal axis using a twin blade saw. The laths and a five-step cellulose calibration wedge are placed on X-ray films and exposed for 14 min. Depth levels of the calibration wedge returned reference values that are used to transform the X-ray film grey-scales into estimates of wood density.

We produced two versions of the Smolikas density record considering two detrending methods to remove biological age trends (Bräker, 1981) from the MXD series: (a) ratios from cubic splines with a 50% frequency-response cutoff at 100 years to emphasize inter-annual to multi-

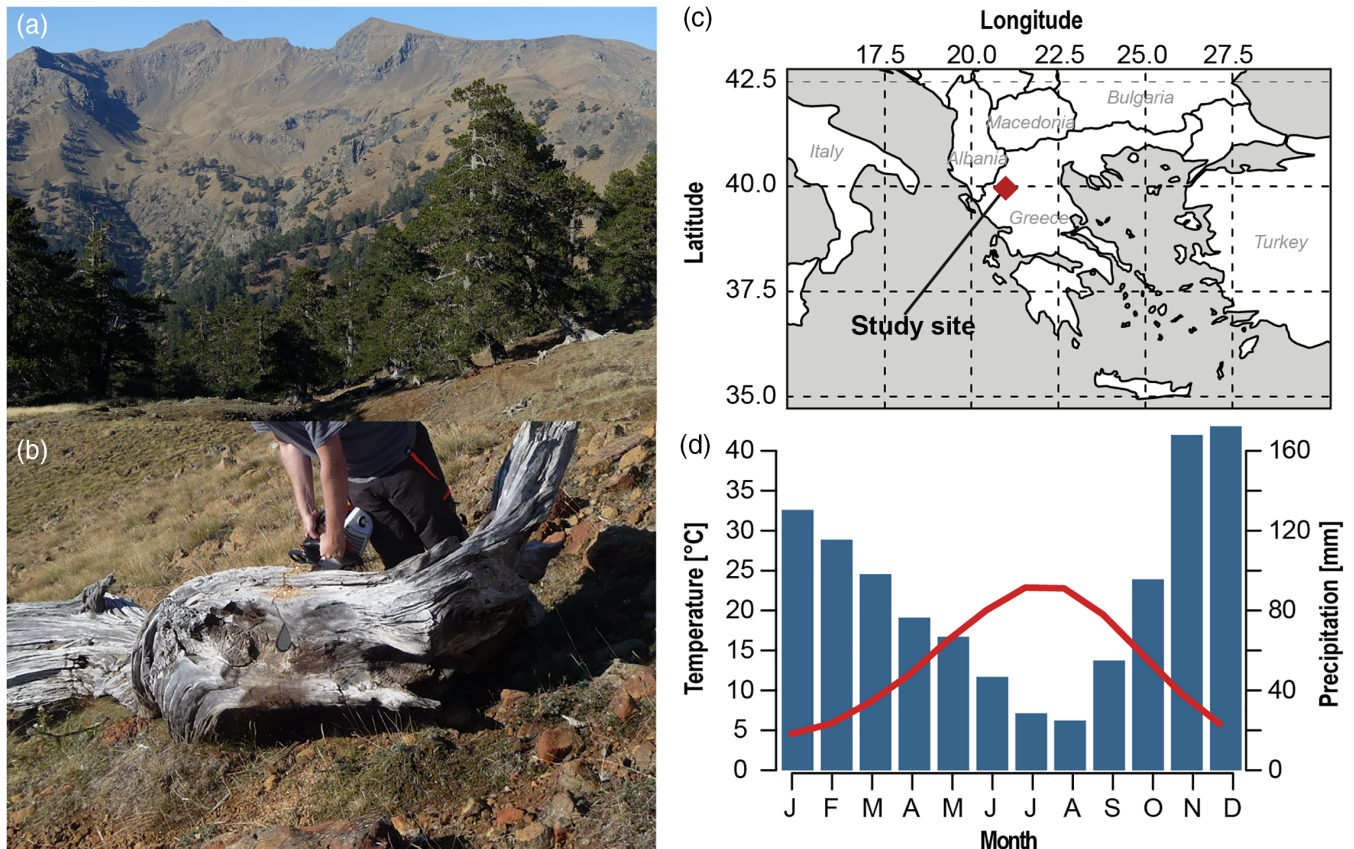


FIGURE 1 Site characteristics. (a) Typical shape of the oro-mediterranean ecotone (2,000–2,200 m a.s.l.) at the eastern foothills of Mt. Smolikas in northwestern Greece with open stands of *Pinus heldreichii* forming the tree-line and (b) sampling of relict material. (c) Map of the of the study region and (d) climate diagram of the meteorological station in Ioannina (39.70°N, 20.80°E, 488 m a.s.l.) for the period 1961–1990 [Colour figure can be viewed at wileyonlinelibrary.com]

decadal scale variability (100SP), and (b) ratios from a spline with a 50% frequency–response cutoff at 10 years to emphasize inter-annual variability (10SP; Cook and Peters, 1981; Cook *et al.*, 2017). These detrendings are specifically designed to preserve high-frequency variance and remove long-term fluctuations. Trends in variance, which mainly originate from changes in sample replication and inter-series correlation (Frank *et al.*, 2007), are corrected by fitting 30-year splines to the mirrored chronologies and calculating ratios (Cook and Peters, 1997). The two (100SP and 10SP) chronologies are truncated at $n < 10$ series. The inter-series correlation (R_{bar}) is calculated using 30-year segments lagged by 15 years to evaluate temporal coherence changes among the MXD series (Wigley *et al.*, 1984). Variance changes are analysed by calculating 100-year moving window SD . In addition, the spline chronologies and absolute density values (g/cm^3) are compared with PIHE MXD data from the nearby Katarapass (KAT) and Mt. Olympus (OLY) in Greece (Klesse *et al.*, 2015), Bulgaria (VIH; Trouet *et al.*, 2012), and Italy (ITP; Schweingruber and Briffa, 1996) (Table 1). Some of these chronologies are available on the ITRDB (<https://www.ncdc.noaa.gov/paleo-search/>; Grissino-Mayer and Fritts, 1997), while others were provided to us by the authors.

2.2 | Climate data and signal detection

The study region is characterized by a Mediterranean climate with warm to hot summers, droughts during June–September, and humid winters (Figure 1d). The distinct intra-annual precipitation differences are caused by seasonal alternations in the occurrence of cyclonic storms in winter and subtropical high-pressure cells in summer (Bolle, 2003). Climate at the elevation of the study site is characterized by cold, snowy winters with snow melt occurring in late spring, and summer dryness is limited to June–August (Fotiadi *et al.*, 1999; Loukas *et al.*, 2002).

The 0.5° gridded EOBS v.15 climate data of the 20.75°E/40.25°N grid point are used for the analysis of growth-climate responses (Haylock *et al.*, 2008). The use of station data (Ioannina Figure 1d, Thessaloniki) and other gridded products (CRU TS 3.24 climate data; Harris *et al.*, 2014) yielded no significant differences in calibration results. As with the MXD data, the temperature data are high-pass filtered by calculating residuals from 100- and 10-year smoothing splines to emphasize inter-annual to decadal scale variance. Growth-climate relationships are assessed by the Pearson correlation coefficients between the chronologies and high-pass filtered temperature and precipitation data for the period 1950–2014, on a monthly basis

TABLE 1 Description and temperature signals of 10 tree-ring maximum latewood density chronologies from Europe used for inter-site comparison of temperature extremes

Code	Site	Country	Species	Length > 10 series	Seasonal target	r 100SP/10SP	EOBS grid Lat°N/Lon°E	Distance
SCA	NScan	Finland	PISY	–4–2006	JJA	0.75/0.75	67–70, 20–28	3,200 km
BRI	Scotland	UK	PISY	1720–1978	JJA	0.75/0.69	47–57, –10–2	2,600 km
PYR	Pyrenees	Spain	PIUN	1229–2014	MJAS	0.65/0.68	42–42.5, 0.5–1	1,800 km
ALP	Lötschental	Switzerl.	LADE	783–2004	JJAS	0.72/0.73	45–47 N, 6–9	1,350 km
TAT	Tatra	Slovakia	LADE	1707–2004	MJJ	0.67/0.74	49–49.5, 20–20.5	1,000 km
ITA	Bosque di Ceppo	Italy	ABAL	1741–1980	AS	0.66/0.74	42.5–43, 13–13.5	700 km
ITP	Sierra de Crispo	Italy	PIHE	1683–1980	JAS	0.54/0.66	39.5–40, 16–16.5	400 km
VIH	Vihren	Bulgaria	PIHE	1769–2008	A	0.67/0.73	41.5–42, 23–23.5	300 km
OLY	Olymp	Greece	PIHE	1530–2010	JAS	0.54/0.60	40–40.5, 22–22.5	100 km
KAT	Katarapass	Greece	PIHE	1759–1981	AS	0.37/0.65	39.5–40, 21–21.5	40 km

Note. Correlation coefficients derived from re-calibration against monthly 100- and 10-year high-pass-filtered EOBS v. 15 gridded temperature data. ABAL: *Abies alba*; Lade: *Larix decidua*; PIHE: *Pinus heldreichii*; PISY: *Pinus sylvestris*; PIUN: *Pinus uncinata*.

and using seasonal windows ranging from previous-year August to current-year October. The pre-1950 instrumental data have previously been shown to be insufficiently reliable for grid interpolations over the mountainous terrain of northern Greece (Klippel *et al.*, 2017; Klippel *et al.*, 2018). Spatial correlation maps were produced using the KNMI Climate Explorer (<https://climexp.knmi.nl/>; Trouet and van Oldenborgh, 2013).

We used a partial correlation approach to distinguish the competing but inter-related influences of precipitation and temperature on MXD formation (Meko *et al.*, 2011). In a first step, simple Pearson correlations between 1- and 2-month windows of temperature or precipitation and the MXD chronologies were calculated. In the second step, a partial correlation was applied removing the effect of the inter-correlation between temperature and precipitation, thereby accentuating the pure temperature or precipitation signal. The stability of the growth-climate relationship for the most important season was tested by modifying sample replication to assess the significance of earlier, less replicated periods of the record (Esper *et al.*, 2012). Correlation coefficients were derived from calibrating a total of 2000 subsamples of the spline chronologies against August–September temperatures. The replicate tree-ring chronologies were developed using 5 to 35 MXD series randomly drawn 2000 times from the population of 43 series that cover the entire calibration period.

2.3 | Reconstruction of temperature extremes

A scaling approach is used for calibration where both the mean and standard deviation of the spline-detrended chronologies are adjusted to their corresponding values of the (spline-detrended) instrumental temperature data to retain the spectrum of instrumental variance in the reconstructions (Esper *et al.*, 2005). Uncertainties in the reconstruction increase back in time due to the decreasing number of series (chronology error), and are estimated in ARSTAN software (Cook *et al.*, 2017) by bootstrapping (Briffa *et al.*, 1992), and transferred into temperature estimates via scaling (Esper

et al., 2007; Trouet, 2014). The reduction of error statistic (RE; Briffa *et al.*, 1988) and coefficient of efficiency (CE; Cook *et al.*, 1994) are used to estimate the strength of the relationship between reconstructed and observed temperatures. Positive RE and CE scores indicate reconstruction skill of the model (Cook *et al.*, 1994). For the detection of extremely cold and warm summers, the ± 1.5 SD threshold is used. Thresholds and detection method are thus unique to every proxy-climate reconstruction experiment and their value affects inter-study comparisons of extremes (Akkemik *et al.*, 2005; Köse *et al.*, 2011; Tejedor *et al.*, 2016). Temporal changes in the frequency of extremes are analysed by counting the numbers of cold and warm events using running 100-year windows.

Superposed epoch analysis (SEA) is performed to quantify post-volcanic cooling over the past millennium (Panofsky and Brier, 1958). We extracted the dates of the 11 largest sulphur peaks in the composite Greenland and Antarctic ice core records (excluding 1458; Sigl *et al.*, 2015), which are thought to be caused by large extra-tropical eruptions as well as the 1835 Cosiguina, 1883 Krakatau (Esper *et al.*, 2013b) and 1452 Kuwae (Esper *et al.*, 2017) eruptions to set the timing of the impulse spike. All SEA results are displayed as temperature anomalies with respect to 5 years prior to the eruptions. Temporal mismatches of 2 years between known and unknown eruptions and reconstructed cooling arise due to dating uncertainties in the ice core sulphur record (Baillie and McAneney, 2015; Schneider *et al.*, 2017).

2.4 | Spatial patterns of temperature extremes

A European-wide comparison of summer temperatures is performed to examine the spatial extent of reconstructed extremes. We compiled a collection of 10 MXD datasets from various locations across Europe including five sites within a 1,000 km radius from the Pindus Mountains (Table 1). All datasets are described as having a clear summer temperature signal, and we accessed the data via the ITRDB or from the original authors. In addition to the four

P. heldreichii chronologies (KAT, OLY, VIH, ITP) detailed above, we added an *Abies alba* (ITA) chronology from Italy (Schweingruber and Briffa, 1996), a *Larix decidua* chronology from the High Tatras in Slovakia (TAT; Büntgen *et al.*, 2007), a *Larix decidua* chronology from the Swiss Alps (ALP; Büntgen *et al.*, 2006), a *Pinus uncinata* chronology from the Pyrenees in Spain (PYR; Büntgen *et al.*, 2017b), a *Pinus sylvestris* regional chronology from 11 sites across British Isles (BRI; Schweingruber and Briffa, 1996; Trouet *et al.*, 2018), and a *Pinus sylvestris* chronology from north Scandinavia (SCA; Esper *et al.*, 2012).

Before comparing the temperature history in our reconstruction with that of the 10 European MXD collections, the raw data in each of the latter are re-standardized and re-calibrated to produce a similar ratio of high-to-low-frequency temperature variability in all datasets (Franke *et al.*, 2013; Esper *et al.*, 2016). Each collection's raw data is standardized according to the methods applied to the SMO dataset (see above). A re-calibration is performed using temperature data from the 0.5° EOBS v.15 dataset (Haylock *et al.*, 2008). The spatial extent of the datasets varies, thus the EOBS temperature grid-size is adjusted to the size of the respective study region described by the chronologies' authors and provided in Table 1. For those datasets previously used for climate reconstruction, seasonal grid-cell means with the highest temperature response is used. For example, the SCA record is calibrated against the mean JJA grid-cell temperatures over the region 67°–70°N and 20°–28°E. All reconstructions are rescaled and extremes are defined as values exceeding ± 1.5 *SD*.

The analysis of synchronous temperature extremes is performed over the common period between the other individual European reconstructions and SMO, as well as the common period 1769–1978 between all reconstructions. Given all the reconstructions differ in their lengths and absolute number of extreme events, the percent overlap is calculated as a mean to enable inter-site comparisons. This analysis is repeated using August temperatures from the EOBS network to explore potential differences between instrumental and tree-ring derived temperature extremes. The analysis is restricted to the month of August to set a comparable time span among different station data. Due to the limited length of instrumental data, and in lieu of the 1.5 *SD* threshold, the five coldest and five warmest instrumental temperature anomalies from each of the 10 calibration time series are compared to the average temperature of the calibration grid-cell (Haylock *et al.*, 2008).

The significance of the number of common events is tested using a bootstrap approach. All reconstructions and instrumental time series were randomized 1,000 times to ensure that extreme events appear by chance over time. This degree of repetition quantifies the range of possible overlaps in extremes that occur in a random time series. A larger number of common extreme years between the unperturbed

reconstructions, compared to the randomized series, indicates common (climatic) forcing.

3 | RESULTS

3.1 | Chronology characteristics

After truncation at a minimum sample replication of $n < 10$ series, the new SMO MXD chronology includes 1277 years and spans the period 738–2014 CE. The number of series changes through time with a minimum of 11 series in 738 CE and a maximum of 44 series in the beginning of the 18th century (Figure 2c). The two detrendings reveal consistent results in the high-frequency domain, but mid-frequency variability only appears in the 100SP chronology (Figure 2a–b). Mean tree age is balanced prior to 1,700 CE and increases towards the present due to the integration of several near millennium-length series (Figure 2d). Coherency among the individual measurement series, expressed by the inter-series correlation (R_{bar}), is moderate with mean R_{bar} values of 0.30 and 0.38 for the 100SP and 10SP chronologies, respectively (Figure 2e). The R_{bar} values indicate the potential to provide high-resolution reconstructions of climate back to the first millennium. The moving *SD*s indicate that variance is stable through time with a general higher *SD* in the 100SP chronology compared to the 10SP chronology resulting from the additionally retained decadal scale variability (Figure 2f).

The spline chronologies correlate significantly at high and mid frequencies with PIHE MXD chronologies from the northeastern Mediterranean. Correlation coefficients range from $r = 0.55$ to 0.82 (Figure S1a–b in Appendix S1, Supporting Information). Absolute density values largely overlap, only the values from the OLY-2010 dataset are significantly lower (Figure S1c in Appendix S1). For the first 200 years of growth, the average MXD per sample is 0.71 g/cm³ and 0.70 g/cm³ during the last 200 years of growth. From the relict material, the values are 0.71 and 0.69 g/cm³, respectively, indicating the material is not significantly affected by weathering processes. Inter-site differences in absolute density values are not significant (Figure S2 in Appendix S1).

3.2 | Climate signals

The SMO record is significantly correlated to temperatures from July to September, with the strongest seasonal response to the August–September mean using the 10SP detrended proxy and instrumental data ($r = 0.71$, $p < .01$; 1950–2014). The correlations are (insignificantly) smaller for the 100SP detrended data ($r = 0.63$), indicating a stronger proxy/temperature coherency at inter-annual time scales. Partial correlation analyses reveal that SMO-MXD data display a pure temperature signal during the summer months,

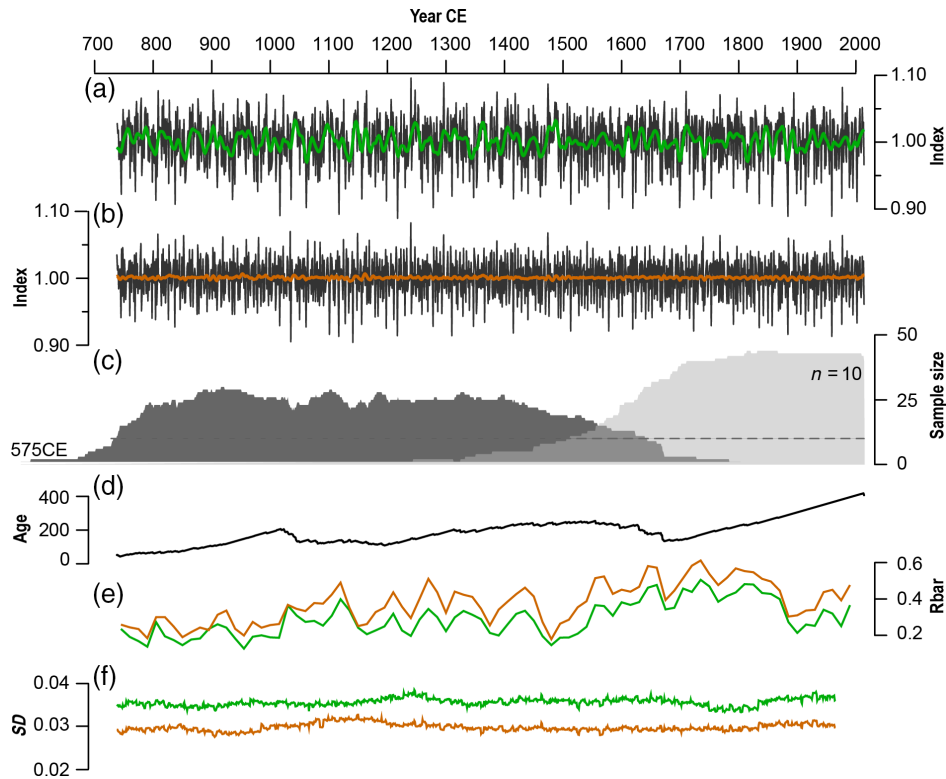


FIGURE 2 Chronology characteristics. (a) 100SP chronology (black) and 15-year smoothed version (green). (b) 10SP chronology (black) and 15-year smoothed version (orange). (c) Yearly sample size for relict (dark grey) and living (light grey) material. (d) Annual mean tree age. (e) Rbar statistics (calculated over 30 years lagged by 15 years) and (f) 100-year moving *SD* for the 100SP chronology (green) and 10SP chronology (orange) [Colour figure can be viewed at wileyonlinelibrary.com]

without artefacts derived from an inter-correlation between temperature and precipitation (Figure S3 in Appendix S1). The recalculation of subsets of 2000, 100SP and 10SP chronologies, and their correlation with August–September temperature, shows that the signal is robust down to a replication of 10 series. The lowest correlation coefficient with a random subset of 10 100SP detrended series is $r = 0.27$ ($p < .05$) and $r = 0.45$ ($p < .001$) for a random subset of 10 10SP series. The lowest replication in the chronology is 11 series, indicating that the less-replicated parts in the early section of the reconstruction likely still contain a statistically significant association with temperature (Figure 3b). Spatial correlations between the spline chronologies and gridded August–September temperatures are also robust, with the highest degree of variance explained by those grid cells closest to the study site (Figure 4). Positive, significant correlation coefficients between MXD indices and August–September temperatures extend from central Italy to western Turkey. Correlations over Austria, Slovenia and Romania are weaker, but still significant. Significantly negative correlation coefficients are found over the British Isles and Scandinavia.

3.3 | Temperature extremes

Results from the calibration/verification exercises indicate a stable growth–climate relationship permitting the use of the

entire 1950–2014 climate record to develop a scaling model for reconstruction. The spline chronologies explain 43 and 51% of the August–September temperature variance over the 1983–2014 calibration period. RE and CE scores for the corresponding 1950–1982 verification period are 0.28 and 0.25 for the 100SP and 0.40 and 0.39 for the 10SP chronology. Transposing the periods, using 1950–1982 for calibration, the 100-year and 10SP chronologies explain 38 and 49% of the August–September temperature variance, RE and CE scores of the corresponding 1983–2014 verification are 0.25 and 0.22 for the 100SP both 0.44 for the 10SP chronology, respectively. Comparison of the August–September temperature trends in both the reconstruction and instrumental data reveals similar inter-annual to decadal scale variance (Figure 3c–d). The three coldest years in the 100SP reconstruction and the four coldest years in the 10SP reconstruction agree with the five coldest measured years, suggesting that both reconstructions contain some skill in capturing temperature extremes.

In total, 110 cold and 48 warm extremes appear in the 100SP reconstruction, and 105 cold and 57 warm extremes in the 10SP reconstruction (Figure 5 and Table S1 in Appendix S1). The year 1240 was the warmest summer, with reconstructed anomalies of $+3.13^{\circ}\text{C}$ and $+2.64^{\circ}\text{C}$ in the 100SP and 10SP reconstructions, respectively. The two coldest summers in the 100SP reconstruction are 1217 and

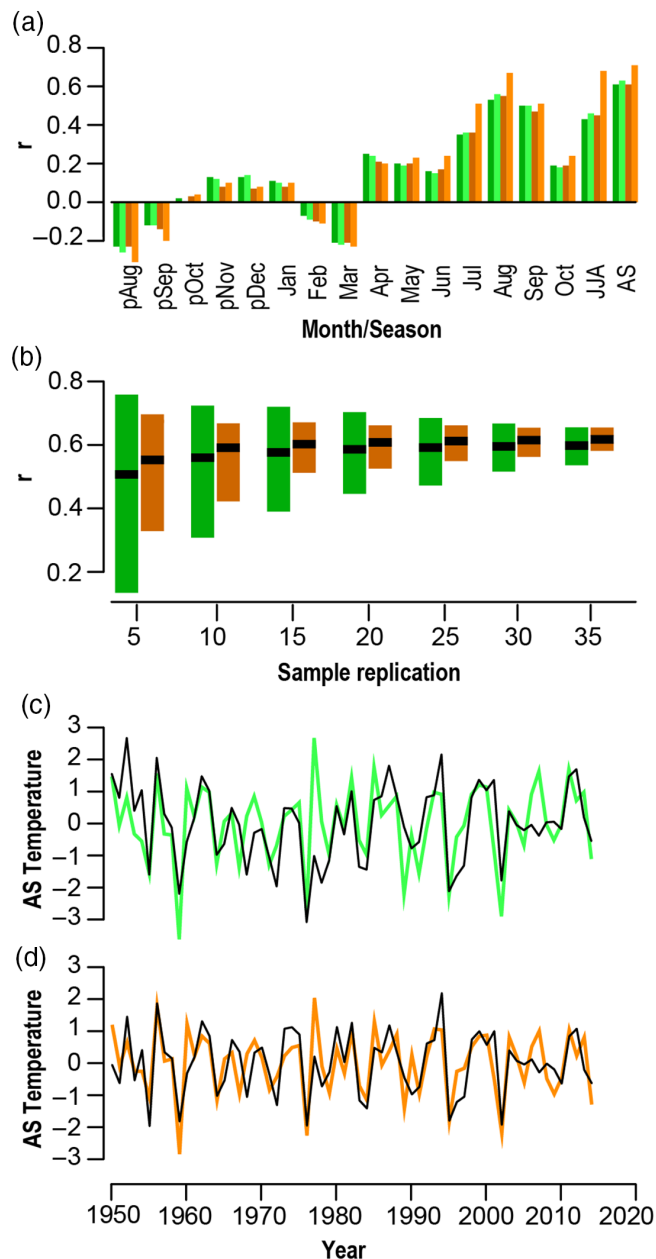


FIGURE 3 Calibration tests. (a) Pearson correlation of the 100SP (dark green), and 10SP (dark orange) chronology with temperature data from the EOBS v.15 grid 40.25°N and 20.75°E for the period 1950–2014 and respective high-pass filtered versions (light green and light orange). (b) Multiple correlation coefficients returned from calibrating a total of 2,000 100SP and 10SP (dark orange) chronologies against August–September temperatures for the period 1950–2014. The 100SP and 10SP chronologies were established randomly selecting from 5 to 35 MXD series from a population of 43 living tree-ring series that span the full calibration period, (c) instrumental 100-year high-pass filtered August–September temperatures (black) and 100SP reconstructed temperatures (light green) and (d) instrumental 10-year high-pass filtered August–September temperatures (black) and 10SP reconstructed temperatures (light orange) [Colour figure can be viewed at wileyonlinelibrary.com]

1884 with anomalies of -3.71°C and -3.61°C , respectively. The two coldest summers in the 10SP reconstruction occurred in different years, 1035 and 1117, with anomalies of -3.11°C and -3.14°C , respectively. The third coldest summer in the 100SP and fourth coldest summer in the

10SP reconstructions, is 1959, which is the second coldest year in the instrumental EOBS v.15 record. The coldest decade is 1811–1820 (-0.73°C) and the warmest decade 1481–1490 ($+0.88^{\circ}\text{C}$; calculated only for 100SP reconstruction). The elimination of decadal trends in the 10SP reconstruction causes events to appear more evenly distributed. However, over the past 450 years the occurrence of warm temperature extremes is substantially less frequent compared to preceding centuries. In contrast, the number of cold extremes moderately increased between 800 and 1,700 CE, rapidly decreased from 1,700 to 1,800 CE, and increased again to the present (Figure 5).

The SEA results suggest that volcanic eruptions are a strong driver of temperature minima (Figure S4 in Appendix S1). In 10 out of 11 cases, a low-temperature anomaly occurred in the year of, or 1 year after, the sulphur peaks in the ice-core record. Years with a significant post-volcanic cooling are 939, 1108, 1171, 1230, 1257, 1453, 1601, 1641, 1695, 1783, 1815, 1835 and 1883. The average temperature response in the first post-volcanic August–September, is -1.72°C to -1.34°C ($p < .01$).

3.4 | Spatial patterns of temperature extremes

Comparison of the temperature extremes in the re-standardized and re-calibrated European records (Figure S5 in Appendix S1) with the SMO-MXD reconstructions reveals two main patterns: (a) for distant sites ($\geq 1,000$ km), the synchronous occurrence of extremes is rare for cold and warm events, and (b) for nearby sites ($< 1,000$ km), the synchronicity is high for cold extremes but moderate to weak for warm extremes (Figure 6). Between the SCA, BRI, PYR, ALP, TAT reconstructions and SMO, the percentage of overlap is 0–14% for cold and 0–6% for warm extremes. Over Britain and Scandinavia (BRI and SCA), we find an inverse relationship. The majority of extreme SMO cold temperature anomalies appears as warm summers in these records. However, the pattern is less distinct for warm extremes (Figure 6a). The common extremes between the ITA, ITP, VIH, OLY, KAT, and SMO reconstructions, over their individual common periods, range between 43 and 56% for cold and 0–27% for warm extremes. Using a bootstrap approach to assess the significance of common inter-series extremes, we find that only the ITP and OLY, and the ITA, VIH and KAT cold extremes occur non-randomly (Figure 6b). Constraining the analysis to the common period 1769–1978 produces similar results (Figure 6c).

Divergence in the spatial scale of warm and cold extremes, which is only visible in tree-ring derived temperature anomalies with cold extremes showing wider synchronicity than warm extremes, is lacking in the instrumental data. Comparison of the synchronicity of the coldest and warmest instrumental temperature anomalies across Europe indicates no differences between cold and warm extremes,

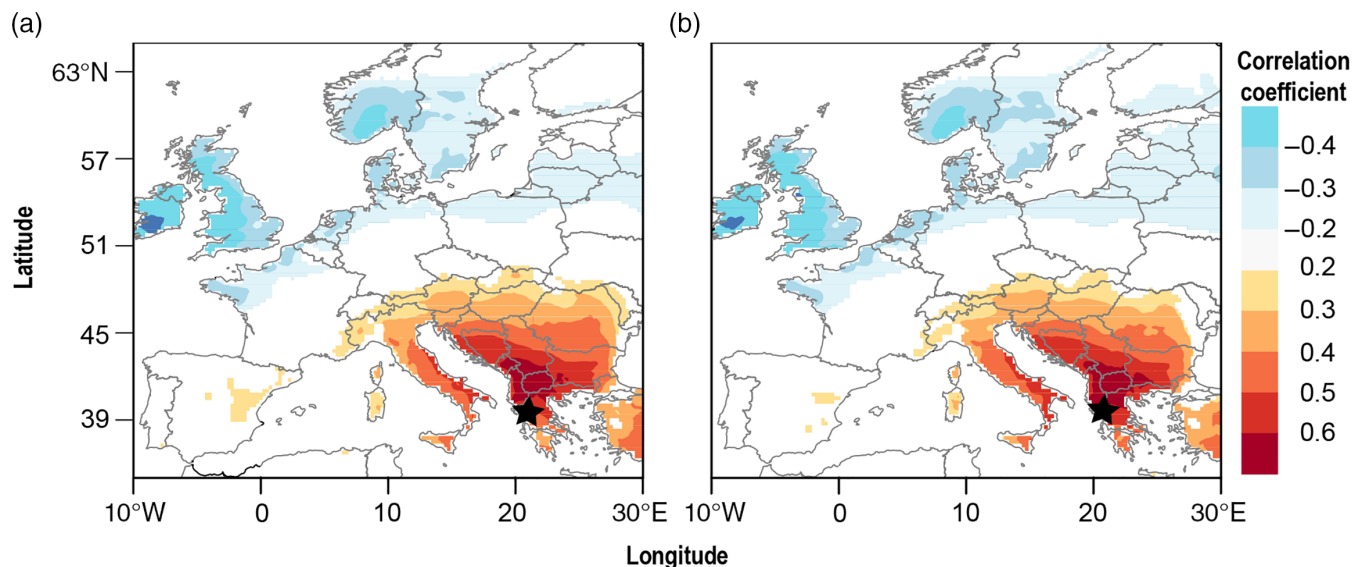


FIGURE 4 Spatial correlation maps ($p < 0.05$) between gridded EOBS v.15 0.25° August–September temperatures and (a) 100SP and (b) 10SP chronologies. Stars refer to the location of the study site [Colour figure can be viewed at wileyonlinelibrary.com]

and with decreasing site distance, the general overlap increases (Figure 6d).

4 | DISCUSSION

Here, we present the longest, annually resolved temperature reconstruction for the Mediterranean region, covering the period 738–2014 CE. Due to the outstanding length, the regional climate history of temperature extremes is extended by roughly 700 years compared to previous temperature reconstructions.

4.1 | Chronology characteristics

At the high-to-mid-frequency range, a strong correlation is found between the SMO spline chronologies and other PIHE records from the central–eastern Mediterranean region, and absolute density levels are in line with previous measurements. Similar values of absolute density between living and relict material (Tegel *et al.*, 2010; Boswijk *et al.*, 2014), and habitat homogeneity (Esper *et al.*, 2016) allows combining the material to extend the SMO chronology back in time. Moderate R_{bar} values point to potential micro-site effects (Düthorn *et al.*, 2013) or tree-specific density variations as a consequence of four differently exposed sites (Figure 1c; Klippel *et al.*, 2017, Klippel *et al.*, 2017). However, absolute values in the range of previous studies from lower altitudes pine trees (Büntgen *et al.*, 2008; Klesse *et al.*, 2015).

4.2 | Climate signals

Partial correlation analysis (Meko *et al.*, 2011) has shown that MXD displays a pure temperature signal that is not affected by the interrelation between temperature and precipitation (Büntgen *et al.*, 2009). Maximum temperature

sensitivity is detected towards the end of the growing season in August and September, which is consistent with the physiological response of cell wall thickening and lignification processes (Fritts, 1976). This response causes cell lumen area to shrink to its minimum and cell wall thickness to increase to its maximum with associated highest MXD values (Cherubini *et al.*, 2004). Similar patterns in climate signal strength in the 100SP and 10SP chronologies suggest that MXD variability is clearly associated with temperature at the mid- and high-frequency.

4.3 | Temperature extremes

In contrast to the multiple climate stations along the Mediterranean that report a general warming in recent decades (Xoplaki *et al.*, 2003a; Alexandrov *et al.*, 2004; Philandras *et al.*, 2008; Toreti *et al.*, 2009), an analysis of instrumental temperatures for the period 1955–2013 shows that in north-western Greece, statistically significant trends in summer temperature are absent (Feidas, 2016). The cooling trend from 1950–1976, previously reported throughout the Mediterranean basin, was followed by an, so far, insignificant warming (Piervitali *et al.*, 1997; del Río *et al.*, 2011). Our reconstruction mirrors this absence of a clear positive trend at decadal scale. Differences in the frequency and magnitude of extreme events between the 100SP and 10SP reconstruction appear because only 76% of the cold, and 65% of the warm events overlap between the two chronology versions. Hence, methods of frequency preservation add uncertainty to the strength of extreme events (Battipaglia *et al.*, 2010). This finding demonstrates how the standardization method employed substantially influences the expression of extremes, thus emphasizes the difficulty in comparing extremes across studies composed of tree-ring data from

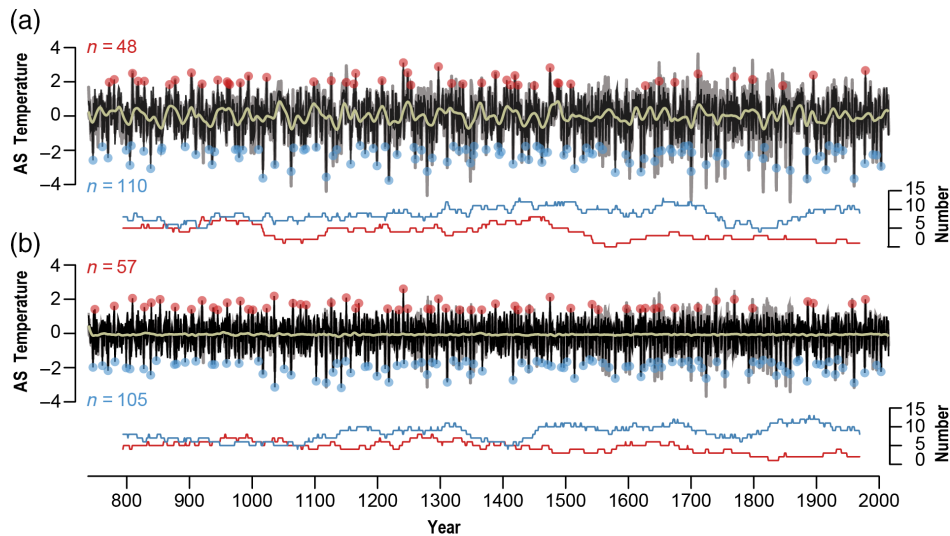


FIGURE 5 Northeastern Mediterranean annually resolved August–September temperatures back to 738 CE and cold (blue) and warm (red) temperature extremes that exceed the threshold of $\pm 1.5 SD$ and corresponding number of extremes in running 100-year windows (lower panels). Panel (a) shows an August–September temperature reconstruction and extremes derived from a 100SP standardized chronology (black), the 15-year smoothed version (yellow) and uncertainty estimates based on the sample bootstrap error (grey) and (b) same for a 10SP chronology [Colour figure can be viewed at wileyonlinelibrary.com]

different sites and, perhaps even, different tree species (Fritts, 1976).

The second coldest decade from 1061–1070 also falls into a period of grand solar minima—the Oort minimum (Guiot *et al.*, 2010). The coldest decade 1811–1820 falls into the periods of the Dalton minimum (Usoskin *et al.*, 2002) and Little Ice Age (Grove, 1988), which coincides with the unknown eruption in 1809 (Guevara-Murua *et al.*, 2014) and the eruption of Tambora in 1815 (Stothers, 1984) causing the “year without summer” 1816 (Oppenheimer, 2003). Cool summers during this decade are also recorded throughout central Europe, parts of Asia and North America by proxy evidence inferred from glacier advances (Luckman, 2000; Zumbühl and Nussbaumer, 2017) and tree-ring data (D’Arrigo *et al.*, 2003; Büntgen *et al.*, 2006; D’Arrigo *et al.*, 2013; Bräuning, 2016), and in long instrumental station data (Böhm *et al.*, 2009). The SEA results demonstrate that several cold summers correspond to volcanic eruptions and changes in radiative forcing (Robock, 2000; Esper *et al.*, 2013a; Esper *et al.*, 2013b). Typical of MXD-based temperature reconstructions (Schneider *et al.*, 2015), the cooling in the first post-volcanic year is followed by a rapid recovery in the second post-volcanic year (Esper *et al.*, 2015). The eruption of Krakatau in 1883 (Sigl *et al.*, 2015) is captured with anomalies of -2.02°C in the 100SP and -0.88°C in the 10SP chronology. Also, the 1257 Samalas (-1.79°C , -1.10°C), 1452 Kuwae (-1.72°C , -1.59°C), 1601 Huaynaputina (-2.70°C , -1.88°C), 1641 Parker (-2.60°C , -2.01°C), 1783 Laki (0.62°C , -1.27°C), 1835 Cosiguina (-2.99°C , -2.43°C), and the 1991 Pinatubo (-1.56°C , -0.98°C) eruptions are related to temperature minima. The 822–823 Katla eruption (Büntgen *et al.*, 2017a) and the unknown eruption in 1809 (Guevara-Murua *et al.*, 2014),

did not cause extreme MXD minima at Mt. Smolikas. The cold summer temperatures in 1699, 1914, and 1857 corroborate reports of previously reported regional climatic extremes (Trouet *et al.*, 2012; Klesse *et al.*, 2015; Leonelli *et al.*, 2017). Instrumental station data in the Mediterranean region (Xoplaki *et al.*, 2003b) confirm the cold summer of 1959 when extremely cool air masses appeared at Mt. Olympus and in Bulgaria. The cold extreme in 1347 (-2.70°C , -2.37°C) coincides to severe plague (*Yersinia pestis*) outbreaks on the Mediterranean islands Sicily, Corsica, and Sardinia as well as well as in the cities Split and Dubrovnik, though a causal link between low temperatures and *Yersinia pestis* seems unlikely (Büntgen *et al.*, 2012).

4.4 | Spatial patterns of temperature extremes

Volcanic eruptions are pulse-like disturbance events capable of causing distinct cooling over Europe (Sigl *et al.*, 2015; Schneider *et al.*, 2017). Despite the Hadley circulation and stable warm high-pressure cells that bring predominantly high temperatures and summer droughts to the Mediterranean (Bolle, 2003; Alfaro-Sánchez *et al.*, 2018), the expression of temperature extremes differs between the northeastern (Pindos Mts.) and western Mediterranean (Pyrenees) basin (Seim *et al.*, 2015). In the western Mediterranean, previous studies report a stronger influence of the East Atlantic jetstream (Düneloh and Jacobeit, 2003; Xoplaki *et al.*, 2003b) and West African Monsoon (Fontaine *et al.*, 2010). By contrast, in the northeastern Mediterranean we find an association with the latitudinal position of the North Atlantic Jet (NAJ) (Mahlstein *et al.*, 2012; Belmecheri *et al.*, 2017; Trouet *et al.*, 2018) that causes temperature extremes and synoptic timing of events in Bulgaria, Italy,

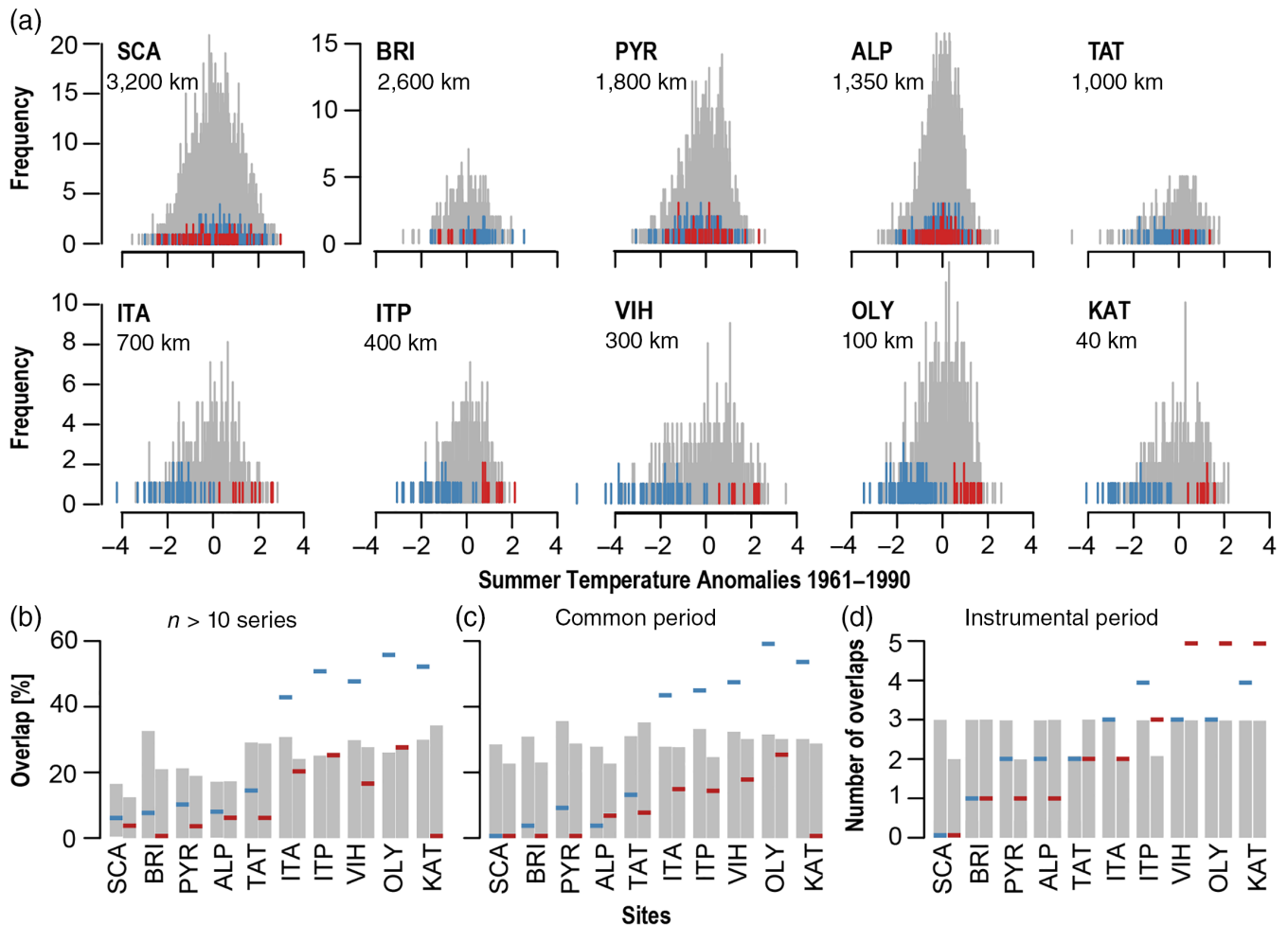


FIGURE 6 Comparison of temperature anomalies and extremes ($\pm 1.5 SD$) across Europe. (a) MXD based 100SP and 10SP temperature reconstructions from Scandinavia (SCA), United Kingdom (BRI), Spain (PYR), Switzerland (ALP), Slovakia (TAT), Italy (ITA and ITP), Bulgaria (VIH), and Greece (OLY and KAT) displayed as histograms (grey). Blue and red ticks indicate cold or warm extremes in the SMO 100SP and 10SP reconstructions and (b) percent of common cold (blue) and (warm) temperature extremes between SMO and the reconstructions displayed in Figure 6 (a) over the individual period of overlap ($n > \text{series}$) and (c) the common period 1769–1978. Values refer to the mean overlap from the 100SP and 10SP reconstruction. Grey bars display uncertainty estimates derived from a Monte Carlo simulation with 1,000 randomized reconstructions. (d) Analysis was repeated comparing the overlap of the 5 coldest and 5 warmest instrumental 10-year high-pass filtered August temperatures from the EOBS v.15 grids that were used for calibration over the period 1950–2014 [Colour figure can be viewed at wileyonlinelibrary.com]

and Greece as well as anti-phase associations with temperature anomalies over Scandinavia and the British Isles (Hughes *et al.*, 2001; Xoplaki *et al.*, 2003b; Oikonomou *et al.*, 2010; Trouet *et al.*, 2012; Trouet, 2014; Klesse *et al.*, 2015). When the NAJ is in anomalously northerly position, it generates anticyclonic conditions in northwestern Europe associated with warm and dry conditions but also heat waves and droughts (Chronis *et al.*, 2011), and extreme cold temperatures in the northeastern Mediterranean. A southerly NAJ increases the blocking frequency over the northeastern Mediterranean and promotes hot summers, droughts, and wildfires in southeastern Europe (Mahlstein *et al.*, 2012; Trouet *et al.*, 2018). To evaluate these associations, the SMO reconstruction is compared to a reconstruction of the latitudinal position of the NAJ (NAJ_T; 1725–1978) developed from tree-ring data from the northeastern Mediterranean (NEMED) and the British Isles (BRIT; Trouet *et al.*, 2018). We used the 100SP SMO reconstruction due to

similar spectral properties of the records (Figure 7). Correlation between the SMO August–September temperature reconstruction and reconstructed NAJ_T anomalies is $r = -0.66$ ($p < .001$).

For validation, we tested the suitability of our SMO dataset for NAJ reconstruction. We repeated the reconstruction NAJ_T procedure outlined in Trouet *et al.* (2018) using our SMO reconstruction in lieu of the NEMED dataset (herein NAJ_K reconstruction). The sole difference involves the use of EOBS v.15 gridded temperature data as a target for reconstruction of August temperatures. The original NEMED MXD chronology and the SMO chronology are significantly correlated with NAJ position ($r = -0.57$ and $r = -0.54$, respectively, $p < .001$; 1920–1978). Also, the original BRIT-NEMED and BRIT-SMO composites reflect changes in the latitudinal position of the NAJ ($r = 0.63$ and $r = 0.59$, respectively, $p < 0.001$; 1920–1978). Reasons that could cause slightly weaker coefficients for SMO include

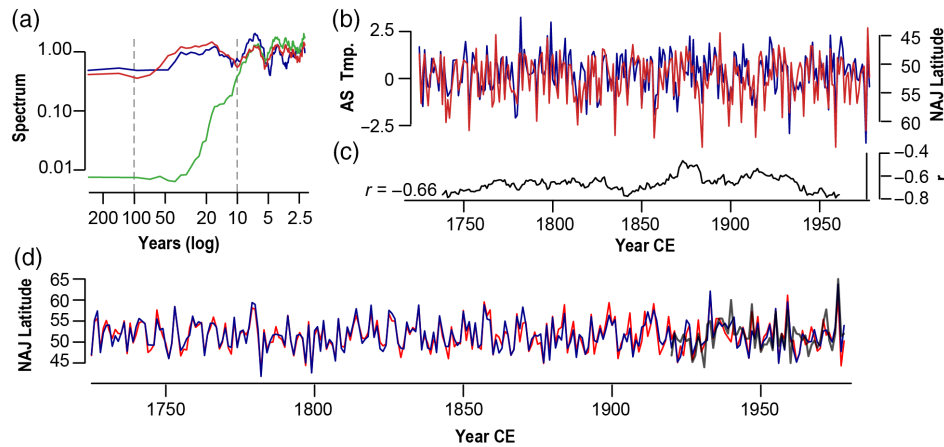


FIGURE 7 (a) Frequency analysis of the SMO 100SP (red), 10SP (green) spline August–September temperature reconstruction and reconstruction of the position of the summer North Atlantic jet (NAJ_T, Trouet *et al.*, 2018) (blue) over the common period 1725–1978. (b) Reconstructed 100SP August–September temperature anomalies (red), summer NAJ_T reconstruction (blue) and (c) corresponding 31-year moving window correlations (black). (d) NAJ_T (blue) and NAJ_K (red), a reanalysis of the latitudinal jet stream position using the SMO tree-ring data instead of the original NEMED compilation and instrumental August NAJ position (black) [Colour figure can be viewed at wileyonlinelibrary.com]

differences in the temperature dataset, reduced sample replication (Esper *et al.*, 2016), and limited spatial representation, as compared to the NEMED data. However, the NAJ_T and NAJ_K reconstructions correlate at $r = 0.9$ ($p < .001$) over their common period 1725–2014 (Figure 7c). This highlights the potential for extending NAJ variability back to the first millennium and forward to the 21st century by including the SMO dataset in future analyses of the temperature seesaw between the British Isles and the northeastern Mediterranean.

4.5 | Differences between warm and cold extremes

Reconstructed warm temperatures are spatially heterogeneous, which we would not expect from the inspection of instrumental data (Figure 6c). We suggest potential weaknesses in MXD to track warm events, due to a decoupling between summer temperature and MXD formation. Except for Scotland, revision of the calibration tests demonstrates that the coldest instrumental temperature anomalies match the lowest density values to a higher degree than the five warmest instrumental temperature anomalies and the highest density values (Figure S6 in Appendix S1). This weakness to track warm extremes by the same degree as cold extremes causes the warm extremes to be less synchronized on a regional scale.

We suggest that in a cold summer, temperature is the limiting factor affecting regional growth (Cherubini *et al.*, 2004), whereas in hot summers, this relationship is more complex with a stronger contribution of endogenous factors affecting cell wall thickening and lignification, causing substantial inter-tree and inter-site differences (Plomion *et al.*, 2001). In addition, slope exposure might influence the rate of warming, which in turn causes a site-specific growth cessation and spatial heterogeneity of warm temperature extremes (Holland and Steyn, 1975; Klippel *et al.*, 2017).

Further research is necessary to disentangle the impact of slope exposure and changes in insolation on MXD formation.

5 | CONCLUSION

Based on a network of high-elevation sites on Mt. Smolikas in the Pindus Mountains of Greece, regional August–September temperature variability is reconstructed back to CE 738. Our reconstruction provides new insight in extreme temperatures in the northeastern Mediterranean prior to the second millennium, and fills a temporal and spatial gap in larger-scale reconstruction efforts. Analysis of temperature extremes shows that cool summers were most severe in 1035, 1117, 1217, 1884 and 1959. The dominant mode that drives annual-decadal temperature variability along the northeastern Mediterranean are atmospheric conditions associated with the position of the NAJ that in the anomalous northward position generates extremely cold summer temperatures in the region, and in an anomalous southward position brings extremely warm summer temperatures. Our new millennium-long MXD chronology bears the potential to reconstruct the dynamics of the NAJ over longer timescales. Further research is needed (1) to explore low-frequency trends including transitions between cold and warm phases, and (2) to update existing regional-scale composite chronologies in order to fill the spatial and temporal gap in the northeastern Mediterranean region in larger-scale temperature reconstructions.

ACKNOWLEDGEMENTS

This research was supported by the German Research Foundation [projects: Inst 247/665-1 FUGG and ES 161/9-1], the National Science Foundation [AGS-1349942], the

Alexander von Humboldt Foundation, and the Swedish Society for Anthropology and *Geography*. We thank Markus Kochbeck, Eileen Kuhl and Philipp Römer for producing MXD measurements, and Claudia Hartl and Robert Brandes for discussion and helpful comments.

CONFLICTS OF INTEREST

The authors declare no conflict of interest.

ORCID

Lara Klippel  <https://orcid.org/0000-0003-3032-7920>

REFERENCES

- Akkemik, U. and Aras, A. (2005) Reconstruction (1689–1994 AD) of April–August precipitation in the southern part of central Turkey. *International Journal of Climatology*, 25, 537–548.
- Akkemik, U., Dagdeviren, N. and Aras, A. (2005) A preliminary reconstruction (A.D. 1635–2000) of spring precipitation using oak tree rings in the western Black Sea region of Turkey. *International Journal of Biometeorology*, 49, 297–302.
- Akkemik, U., D'Arrigo, R., Cherubini, P., Köse, N. and Jacoby, G.C. (2008) Tree-ring reconstructions of precipitation and streamflow for north-western Turkey. *International Journal of Climatology*, 28, 173–183.
- Alexandrov, V., Schneider, M., Koleva, E. and Moisselin, J.M. (2004) Climate variability and change in Bulgaria during the 20th century. *Theoretical and Applied Climatology*, 79, 33–149.
- Alfaro-Sánchez, R., Nguyen, H., Klesse, S., Hudson, A., Belmecheri, S., Köse, N., Diaz, H.F., Monson, R.K., Villalba, R. and Trouet, V. (2018) Natural drivers of spring northern tropical belt movements over the past 800 years. *Nature Geoscience*, 11, 933–938. <https://doi.org/10.1038/s41561-018-0242-1>.
- Alpert, P. (2002) The paradoxical increase of Mediterranean extreme daily rainfall in spite of decrease in total values. *Geophysical Research Letters*, 29, 1536. <https://doi.org/10.1029/2001GL013554>.
- Baillie, M.G.L. and McAneney, J. (2015) Tree ring effects and ice core acidities clarify the volcanic record of the first millennium. *Climate of the Past*, 11, 105–114.
- Battipaglia, G., Frank, D., Büntgen, U., Dobrovolný, P., Brázdil, R., Pfister, C. and Esper, J. (2010) Five centuries of Central European temperature extremes reconstructed from tree-ring density and documentary evidence. *Global and Planetary Change*, 72, 182–191.
- Belmecheri, S., Babst, F., Hudson, A.R., Betancourt, J. and Trouet, V. (2017) Northern hemisphere jet stream position indices as diagnostic tools for climate and ecosystem dynamics. *Earth Interactions*, 21, 1–23.
- Böhm, R., Jones, P.D., Hiebl, J., Frank, D., Brunetti, M. and Maugeri, M. (2009) The early instrumental warm-bias: a solution for long central European temperature series 1760–2007. *Climatic Change*, 101, 41–67.
- Bolle, H.J. (2003) *Mediterranean Climate*. Heidelberg, Germany: Springer.
- Boswijk, G., Fowler, A.M., Palmer, J.G., Fenwick, P., Hogg, A., Lorrey, A. and Wunder, J. (2014) The late Holocene kauri chronology: assessing the potential of a 4500-year record for palaeoclimate reconstruction. *Quaternary Science Reviews*, 90, 128–142.
- Bräker, O.U. (1981) Der Alterstrend bei Jahringdichten und Jahringbreiten von Nadelhölzern und sein Ausgleich. *Mitteilungen der Forstlichen Bundesversuchsanstalt Wien*, 142, 75–102.
- Bräuning, A. (2016) Tree-ring evidence of 'Little Ice Age' glacier advances in southern Tibet. *The Holocene*, 16, 369–380.
- Briffa, K.R., Jones, P.D., Pilcher, J.R. and Hughes, M.K. (1988) Reconstructing summer temperatures in northern Fennoscandia back to AD 1700 using tree-ring data from Scots pine. *Arctic, Antarctic, and Alpine Research*, 20, 385–394.
- Briffa, K.R., Jones, P.D., Bartholin, T.S., Eckstein, D., Schweingruber, F.H., Karlen, W., Zetterberg, P. and Eronen, M. (1992) Fennoscandian summers from AD 500—temperature changes on short and long timescales. *Climate Dynamics*, 7, 111–119.
- Büntgen, U., Frank, D.C., Nievergelt, D. and Esper, J. (2006) Summer temperature variations in the European Alps, AD 755–2004. *Journal of Climate*, 19, 5606–5623.
- Büntgen, U., Frank, D.C., Kaczka, R.J., Verstege, A., Zwijacz-Kozica, T. and Esper, J. (2007) Growth responses to climate in a multi-species tree-ring network in the Western Carpathian Tatra Mountains, Poland and Slovakia. *Tree Physiology*, 27, 689–702.
- Büntgen, U., Frank, D., Grudd, H. and Esper, J. (2008) Long-term summer temperature variations in the Pyrenees. *Climate Dynamics*, 31, 615–631.
- Büntgen, U., Frank, D., Trouet, V. and Esper, J. (2009) Diverse climate sensitivity of Mediterranean tree-ring width and density. *Trees*, 24, 261–273.
- Büntgen, U., Tegel, W., Nicolussi, K., McCormick, M., Frank, D., Trouet, V., Kaplan, J.O., Herzig, F., Heussner, K.U., Wanner, H., Luterbacher, J. and Esper, J. (2011) 2500 years of European climate variability and human susceptibility. *Science*, 331, 578–582.
- Büntgen, U., Ginzler, C., Esper, J., Tegel, W. and McMichael, A.J. (2012) Digitizing historical plague. *Clinical Infectious Diseases*, 55, 1586–1588.
- Büntgen, U., Eggertsson, O., Wacker, L., Sigl, M., Ljungqvist, F.C., Di Cosmo, N., Plunkett, G., Krusic, P.J., Newfield, T.P., Esper, J., Lane, C., Reinig, F. and Oppenheimer, C. (2017a) Multi-proxy dating of Iceland's major pre-settlement Katla eruption to 822–823 CE. *Geology*, 45, 783–786.
- Büntgen, U., Krusic, P.J., Verstege, A., Sangüesa-Barreda, G., Wagner, S., Camarero, J.J., Ljungqvist, F.C., Zorita, E., Oppenheimer, C., Konter, O., Tegel, W., Gärtner, H., Cherubini, P., Reinig, F. and Esper, J. (2017b) New tree-ring evidence from the Pyrenees reveals western Mediterranean climate variability since medieval times. *Journal of Climate*, 30, 5295–5318.
- Camuffo, D., Bertolin, C., Barriendos, M., Dominguez-Castro, F., Cocheo, C., Enzi, S., Sghedoni, M., della Valle, A., Garnier, E., Alcoforado, M.J., Xoplaki, E., Luterbacher, J., Diodato, N., Maugeri, M., Nunes, M.F. and Rodriguez, R. (2010) 500-year temperature reconstruction in the Mediterranean Basin by means of documentary data and instrumental observations. *Climatic Change*, 101, 169–199.
- Cherubini, P., Gärtner, H., Esper, J., Dobbertin, M.K., Kaiser, K.F., Rigling, A., Treydte, K., Zimmermann, N.E. and Bräker, O.U. (2004) Jahrringe als Archive für interdisziplinäre Umweltforschung | Annual rings as an archive for interdisciplinary environmental research. *Schweizerische Zeitschrift für Forstwesen*, 155, 162–168.
- Chronis, T., Raitsos, D.E., Kassis, D. and Sarantopoulos, A. (2011) The summer North Atlantic Oscillation influence on the eastern Mediterranean. *Journal of Climate*, 24, 5584–5596.
- Cook, E.R. and Peters, K. (1981) The smoothing spline: a new approach to standardizing forest interior tree-ring width series for dendroclimatic studies. *Tree Ring Bulletin*, 41, 45–53.
- Cook, E.R., Briffa, K.R. and Jones, P.D. (1994) Spatial regression methods in dendroclimatology: a review and comparison of two techniques. *International Journal of Climatology*, 14, 379–402.
- Cook, E. and Peters, K. (1997) Calculating unbiased tree-ring indices for the study of climatic and environmental change. *Holocene*, 7, 361–370.
- Cook, E., Krusic, P.J., Peters, K., and Holmes, R.L.. 2017. *Program ARSTAN version48d2, Autoregressive tree-ring standardization program*. Tree-Ring Laboratory of Lamot-Doherty Earth Observatory. Available at: <http://www.ideo.columbia.edu/tree-ring-laboratory/resources/software> [Accessed 30th March 2018].
- D'Arrigo, R., Buckley, B., Kaplan, S. and Woollett, J. (2003) Interannual to multidecadal modes of Labrador climate variability inferred from tree rings. *Climate Dynamics*, 20, 219–228.
- D'Arrigo, R., Wilson, R. and Anchukaitis, K.J. (2013) Volcanic cooling signal in tree ring temperature records for the past millennium. *Journal of Geophysical Research—Atmospheres*, 118, 9000–9010.
- del Río, S., Herrero, L., Pinto-Gomes, C. and Penas, A. (2011) Spatial analysis of mean temperature trends in Spain over the period 1961–2006. *Global and Planetary Change*, 78, 65–75.
- Diffenbaugh, N.S., Pal, J.S., Giorgi, F. and Gao, X.J. (2007) Heat stress intensification in the Mediterranean climate change hotspot. *Geophysical Research Letters*, 34, L11706. <https://doi.org/10.1029/2007GL030000>.
- Dorado Liñán, I., Büntgen, U., González-Rouco, F., Zorita, E., Montávez, J.P., Gómez-Navarro, J.J., Brunet, M., Heinrich, I., Helle, G. and Gutiérrez, E. (2012) Estimating 750 years of temperature variations and uncertainties in the Pyrenees by tree-ring reconstructions and climate simulations. *Climate of the Past*, 8, 919–933.

- Dükeloh, A. and Jacobeit, J. (2003) Circulation dynamics of Mediterranean precipitation variability 1948–98. *International Journal of Climatology*, 23, 1843–1866.
- Düthorn, E., Holzkämper, S., Timonen, M. and Esper, J. (2013) Influence of micro-site conditions on tree-ring climate signals and trends in central and northern Sweden. *Trees*, 27, 1395–1404.
- Esper, J., Frank, D., Wilson, R. and Briffa, K.R. (2005) Effect of scaling and regression on reconstructed temperature amplitude for the past millennium. *Geophysical Research Letters*, 32, L07711. <https://doi.org/10.1029/2004GL021236>.
- Esper, J., Frank, D., Büntgen, U., Verstege, A. and Luterbacher, J. (2007) Long-term drought severity variations in Morocco. *Geophysical Research Letters*, 34, L17702. <https://doi.org/10.1029/2007GL030844>.
- Esper, J., Büntgen, U., Timonen, M. and Frank, D.C. (2012) Variability and extremes of northern Scandinavian summer temperatures over the past two millennia. *Global and Planetary Change*, 88–89, 1–9.
- Esper, J., Büntgen, U., Luterbacher, J. and Krusic, P.J. (2013a) Testing the hypothesis of post-volcanic missing rings in temperature sensitive dendrochronological data. *Dendrochronologia*, 31, 216–222.
- Esper, J., Schneider, L., Krusic, P.J., Luterbacher, J., Büntgen, U., Timonen, M., Sirocko, F. and Zorita, E. (2013b) European summer temperature response to annually dated volcanic eruptions over the past nine centuries. *Bulletin of Volcanology*, 75, 736.
- Esper, J., Düthorn, E., Krusic, P.J., Timonen, M. and Büntgen, U. (2014a) Northern European summer temperature variations over the Common Era from integrated tree-ring density records. *Journal of Quaternary Science*, 29, 487–494.
- Esper, J., Großjean, J., Camarero, J.J., García-Cervigón, A.I., Olano, J.M., González-Rouco, J.F., Domínguez-Castro, F. and Büntgen, U. (2014b) Atlantic and Mediterranean synoptic drivers of central Spanish juniper growth. *Theoretical and Applied Climatology*, 121, 571–579.
- Esper, J., Schneider, L., Smerdon, J.E., Schöne, B.R. and Büntgen, U. (2015) Signals and memory in tree-ring width and density data. *Dendrochronologia*, 35, 62–70.
- Esper, J., Krusic, P.J., Ljungqvist, F.C., Luterbacher, J., Carrer, M., Cook, E., Davi, N.K., Hartl-Meier, C., Kirilyanov, A., Konter, O., Myglan, V., Timonen, M., Treyde, K., Trouet, V., Villalba, R., Yang, B. and Büntgen, U. (2016) Ranking of tree-ring based temperature reconstructions of the past millennium. *Quaternary Science Reviews*, 145, 134–151.
- Esper, J., Büntgen, U., Hartl-Meier, C., Oppenheimer, C. and Schneider, L. (2017) Northern Hemisphere temperature anomalies during the 1450s period of ambiguous volcanic forcing. *Bulletin of Volcanology*, 79, 41.
- Feidas, H. (2016) Trend analysis of air temperature time series in Greece and their relationship with circulation using surface and satellite data: recent trends and an update to 2013. *Theoretical and Applied Climatology*, 129, 1383–1406.
- Fontaine, B., Garcia-Serrano, J., Roucou, P., Rodriguez-Fonseca, B., Losada, T., Chauvin, F., Gervois, S., Sijikumar, S., Ruti, P. and Janicot, S. (2010) Impacts of warm and cold situations in the Mediterranean basins on the West African monsoon: observed connection patterns (1979–2006) and climate simulations. *Climate Dynamics*, 35, 95–114.
- Fotiadi, A.K., Metaxas, D.A. and Bartzokas, A. (1999) A statistical study of precipitation in Northwest Greece. *International Journal of Climatology*, 19, 1221–1232.
- Frank, D., Esper, J. and Cook, E.R. (2007) Adjustment for proxy number and coherence in a large-scale temperature reconstruction. *Geophysical Research Letters*, 34, L16709. <https://doi.org/10.1029/2007GL030571>.
- Franke, J., Frank, D., Raible, C.C., Esper, J. and Bronnimann, S. (2013) Spectral biases in tree-ring climate proxies. *Nature Climate Change*, 3, 360–364.
- Fritts, H.C. (1976) *Tree Rings and Climate*. Caldwell, ID: Blackburn Press.
- García-Herrera, R., Hernández, E., Barriopedro, D., Paredes, D., Trigo, R.M., Trigo, I.F. and Mendes, M.A. (2007) The outstanding 2004/05 drought in the Iberian Peninsula: associated atmospheric circulation. *Journal of Hydro-meteorology*, 8, 483–498.
- Gogou, A., Triantaphyllou, M., Xoplaki, E., Izdebski, A., Parinos, C., Dimiza, M., Bouloubassi, I., Luterbacher, J., Kouli, K., Martrat, B., Toreti, A., Fleitmann, D., Rousakis, G., Kaberi, H., Athanasiou, M. and Lykousis, V. (2016) Climate variability and socio-environmental changes in the northern Aegean (NE Mediterranean) during the last 1500 years. *Quaternary Science Reviews*, 136, 209–228.
- Grauel, A.L., Leider, A., Goudeau, M.L.S., Müller, I.A., Bernasconi, S.M., Hinrichs, K.U., de Lange, G.J., Zonneveld, K.A.F. and Versteegh, G.J.M. (2013) What do SST proxies really tell us? A high-resolution multiproxy (UK'37, TEXH86 and foraminifera $\delta^{18}O$) study in the Gulf of Taranto, central Mediterranean Sea. *Quaternary Science Reviews*, 73, 115–131.
- Griggs, C., DeGaetano, A., Kuniholm, P. and Newton, M. (2007) A regional high-frequency reconstruction of May–June precipitation in the north Aegean from oak tree rings, AD 1089–1989. *International Journal of Climatology*, 27, 1075–1089.
- Grissino-Mayer, H.D. and Fritts, H.C. (1997) The International Tree-Ring Data Bank: an enhanced global database serving the global scientific community. *Holocene*, 7, 235–238.
- Grove, J.M. (1988) *The Little Ice Age*. New York, NY: Methuen & Co.
- Guevara-Murua, A., Williams, C.A., Hendy, E.J., Rust, A.C. and Cashman, K.V. (2014) Observations of a stratospheric aerosol veil from a tropical volcanic eruption in December 1808: is this the unknown ~ 1809 eruption? *Climate of the Past*, 10, 1707–1722.
- Guiot, J., Corona, C. and members, E.S.C.A.R.S.E.L. (2010) Growing season temperatures in Europe and climate forcings over the past 1400 years. *PLoS One*, 5, e9972. <https://doi.org/10.1371/journal.pone.0009972>.
- Harris, I., Jones, P.D., Osborn, T.J. and Lister, D.H. (2014) Updated high-resolution grids of monthly climatic observations—the CRU TS3.10. *International Journal of Climatology*, 34, 623–642.
- Haylock, M.R., Hofstra, N., Tank, A., Klok, E.J., Jones, P.D. and New, M. (2008) A European daily high-resolution gridded data set of surface temperature and precipitation for 1950–2006. *Journal of Geophysical Research—Atmospheres*, 113, D20119. <https://doi.org/10.1029/2008JD010201>.
- Hoerling, M., Eischeid, J., Perlwitz, J., Quan, X., Zhang, T. and Pegion, P. (2012) On the increased frequency of Mediterranean drought. *Journal of Climate*, 25, 2146–2161.
- Holland, P.G. and Steyn, D.G. (1975) Vegetational responses to latitudinal variations in slope angle and aspect. *Journal of Biogeography*, 2, 179–183.
- Hughes, M.K., Kuniholm, P.I., Eischeid, J.K., Garfin, G., Griggs, C.B. and Latini, C. (2001) Aegean tree-ring signature years explained. *Tree Ring Res.*, 57, 67–73.
- Izdebski, A., Koloch, G. and Słoczyński, T. (2016) Exploring Byzantine and Ottoman economic history with the use of palynological data: a quantitative approach. *Jahrbuch der Österreichischen Byzantinistik*, 1, 67–110.
- Kiss, A., Wilson, R. and Bariska, I. (2011) An experimental 392-year documentary-based multi-proxy (vine and grain) reconstruction of May–July temperatures for Koszeg, West-Hungary. *International Journal of Biometeorology*, 55, 595–611.
- Klesse, S., Ziehmer, M., Rousakis, G., Trouet, V. and Frank, D. (2015) Synoptic drivers of 400 years of summer temperature and precipitation variability on Mt. Olympus, Greece. *Climate Dynamics*, 45, 807–824.
- Klippel, L., Krusic, P.J., Brandes, R., Hartl-Meier, C., Trouet, V., Meko, M. and Esper, J. (2017) High-elevation inter-site differences in Mount Smolikas tree-ring width data. *Dendrochronologia*, 44, 164–173.
- Klippel, L., Krusic, P.J., Brandes, R., Hartl, C., Belmecheri, S., Dienst, M. and Esper, J. (2018) A 1286-year hydro-climate reconstruction for the Balkan Peninsula. *Boreas (Online Version before inclusion in an issue)*, 47, 1218–1229. <https://doi.org/10.1111/bor.12320>.
- Köse, N., Akkemik, Ü., Dalfes, H.N. and Özeren, M.S. (2011) Tree-ring reconstructions of May–June precipitation for western Anatolia. *Quaternary Research*, 75, 438–450.
- Kostopoulou, E. and Jones, P.D. (2005) Assessment of climate extremes in the Eastern Mediterranean. *Meteorology and Atmospheric Physics*, 89, 69–85.
- Kuglitsch, F.G., Toreti, A., Xoplaki, E., Della-Marta, P.M., Zerefos, C.S., Turkes, M. and Luterbacher, J. (2010) Heat wave changes in the eastern Mediterranean since 1960. *Geophysical Research Letters*, 37, L04802. <https://doi.org/10.1029/2009GL041841>.
- Lelieveld, J., Hadjinicolaou, P., Kostopoulou, E., Giannakopoulos, C., Pozzer, A., Tanarhte, M. and Tyrllis, E. (2013) Model projected heat extremes and air pollution in the eastern Mediterranean and Middle East in the twenty-first century. *Regional Environmental Change*, 14, 1937–1949.
- Lenz, O., Schär, E. and Schweingruber, F.H. (1976) Methodische Probleme bei der radiographisch-densitometrischen Bestimmung der Dichte und der Jahrringbreiten von Holz. *Holzforschung*, 30, 114–123.
- Leonelli, G., Coppola, A., Salvatore, M.C., Baroni, C., Battipaglia, G., Gentilesca, T., Ripullone, F., Borghetti, M., Conte, E., Tognetti, R., Marchetti, M., Lombardi, F., Brunetti, M., Maugeri, M., Pelfini, M.,

- Cherubini, P., Provenzale, A. and Maggi, V. (2017) Climate signals in a multispecies tree-ring network from central and southern Italy and reconstruction of the late summer temperatures since the early 1700s. *Climate of the Past*, 13, 1451–1471.
- Levanic, T., Popa, I., Poljansek, S. and Nechita, C. (2012) A 323-year long reconstruction of drought for SW Romania based on black pine (*Pinus Nigra*) tree-ring widths. *International Journal of Biometeorology*, 57, 703–714.
- Li, L., Casado, A., Congedi, L., Dell'Aquila, A., Dubois, C., Elizalde, A., L'Hévéder, B., Lionello, P., Sevaut, F., Somot, S., Ruti, P. and Zampieri, M. (2012) Modeling of the mediterranean climate system. In: Lionello, P. (Ed.) *The Climate of the Mediterranean Region from the Past to the Future*. Lecce: Elsevier, pp. 419–448.
- Linderholm, H.W., Björklund, J., Seftigen, K., Gunnarson, B.E. and Fuentes, M. (2014) Fennoscandia revisited: a spatially improved tree-ring reconstruction of summer temperatures for the last 900 years. *Climate Dynamics*, 45, 933–947.
- Ljungqvist, F.C., Krusic, P.J., Sundqvist, H.S., Zorita, E., Brattstrom, G. and Frank, D. (2016) Northern Hemisphere hydroclimate variability over the past twelve centuries. *Nature*, 532, 94–98.
- Loukas, A., Vasilades, L. and Dalezios, N.R. (2002) Hydroclimatic variability of regional droughts in Greece using the palmer moisture anomaly index. *Nordic Hydrology*, 33, 425–442.
- Luckman, B.H. (2000) The little ice age in the Canadian Rockies. *Geomorphology*, 32, 357–384.
- Mahlstein, I., Martius, O., Chevalier, C. and Ginsbourger, D. (2012) Changes in the odds of extreme events in the Atlantic basin depending on the position of the extratropical jet. *Geophysical Research Letters*, 39, L22805. <https://doi.org/10.1029/2012GL053993>.
- Meko, D.M., Touchan, R. and Anchukaitis, K.J. (2011) Seascorr: a MATLAB program for identifying the seasonal climate signal in an annual tree-ring time series. *Computers & Geosciences*, 37, 1234–1241.
- Melvin, T.M., Grudd, H. and Briffa, K.R. (2013) Potential bias in 'updating' tree-ring chronologies using regional curve standardisation: re-processing 1500 years of Torneträsk density and ring-width data. *Holocene*, 23, 364–373.
- Moriondo, M., Good, P., Durao, R., Bindi, M., Giannakopoulos, C. and Corte-Real, J. (2006) Potential impact of climate change on fire risk in the Mediterranean area. *Climate Research*, 31, 85–95.
- Oikonomou, C., Flocas, H.A., Hatzaki, M., Nisantzi, A. and Asimakopoulos, D. N. (2010) Relationship of extreme dry spells in Eastern Mediterranean with large-scale circulation. *Theoretical and Applied Climatology*, 100, 137–151.
- Oppenheimer, C. (2003) Climatic, environmental and human consequences of the largest known historic eruption: Tambora volcano (Indonesia) 1815. *Progress in Physical Geography*, 27, 230–259.
- Pages 2k PMIP3 Group. (2015) Continental-scale temperature variability in PMIP3 simulations and PAGES 2k regional temperature reconstructions over the past millennium. *Geophysical Research Letters*, 11, 1673–1699.
- Panofsky, H.A. and Brier, G.W. (1958) *Some Applications of Statistics to Meteorology*. University Park, PA: College of Earth and Mineral Sciences.
- Philandras, C.M., Nastos, P.T. and Repapis, C.C. (2008) Air temperature variability and trends over Greece. *Global NEST Journal*, 10, 273–285.
- Piervitali, E., Colacino, M. and Conte, M. (1997) Signals of climatic change in the Central-Western Mediterranean basin. *Theoretical and Applied Climatology*, 58, 211–219.
- Plomion, C., Leprovost, G. and Stokes, A. (2001) Wood formation in trees. *Plant Physiology*, 127, 1513–1523.
- Robock, A. (2000) Volcanic eruptions and climate. *Reviews of Geophysics*, 38, 191–219.
- Schneider, L., Smerdon, J.E., Büntgen, U., Wilson, R., Myglan, V.S., Kirilyanov, A.V. and Esper, J. (2015) Revising midlatitude summer temperatures back to AD 600 based on a wood density network. *Geophysical Research Letters*, 42, 4556–4562.
- Schneider, L., Smerdon, J.E., Pretis, F., Hartl-Meier, C. and Esper, J. (2017) A new archive of large volcanic events over the past millennium derived from reconstructed summer temperatures. *Environmental Research Letters*, 12, 119501. <https://doi.org/10.1088/1748-9326/aa9426>.
- Schweingruber, F.H., Fritts, H.C., Bräker, O.U., Drew, L.G. and Schär, E. (1978) The X-ray technique as applied to dendroclimatology. *Tree Ring Bulletin*, 38, 61–91.
- Schweingruber, F.H., Bartholin, T., Schaur, E. and Briffa, K.R. (1988) Radiodensitometric-dendroclimatological conifer chronologies from Lapland (Scandinavia) and the Alps (Switzerland). *Boreas*, 17, 559–566.
- Schweingruber, F.H. and Briffa, K.R. (1996) Tree-ring density networks for climate reconstruction. In: Jones, P.D., Bradley, R.S. and Jouzel, J. (Eds.) *Climatic Variations and Forcing Mechanisms of the Last 2000 Years*. Heidelberg, Germany: Springer, pp. 43–66.
- Seim, A., Büntgen, U., Fonti, P., Haska, H., Herzig, F., Tegel, W., Trouet, V. and Treydte, K. (2012) Climate sensitivity of a millennium-long pine chronology from Albania. *Climate Research*, 51, 217–228.
- Seim, A., Treydte, K., Trouet, V., Frank, D., Fonti, P., Tegel, W., Panayotov, M., Fernandez-Donado, L., Krusic, P. and Büntgen, U. (2015) Climate sensitivity of Mediterranean pine growth reveals distinct east-west dipole. *International Journal of Climatology*, 35, 2503–2513.
- Sigl, M., Winstrup, M., McConnell, J.R., Welten, K.C., Plunkett, G., Ludlow, F., Büntgen, U., Caffee, M., Chellman, N., Dahl-Jensen, D., Fischer, H., Kipfstuhl, S., Kostick, C., Maselli, O.J., Mekhaldi, F., Mulvaney, R., Muscheler, R., Pasteris, D.R., Pilcher, J.R., Salzer, M., Schupbach, S., Steffensen, J.P., Vinther, B.M. and Woodruff, T.E. (2015) Timing and climate forcing of volcanic eruptions for the past 2,500 years. *Nature*, 523, 543–549.
- Sousa, P.M., Trigo, R.M., Aizpurua, P., Nieto, R., Gimeno, L. and Garcia-Herrera, R. (2011) Trends and extremes of drought indices throughout the 20th century in the Mediterranean. *Natural Hazards and Earth System Sciences*, 11, 33–51.
- Spinoni, J., Naumann, G., Vogt, J. and Barbosa, P. (2015) European drought climatologies and trends based on a multi-indicator approach. *Global and Planetary Change*, 127, 50–57.
- Stothers, R.B. (1984) The great tabora eruption in 1815 and its aftermath. *Science*, 224, 1191–1198.
- Tegel, W., Vanmoerkerke, J. and Büntgen, U. (2010) Updating historical tree-ring records for climate reconstruction. *Quaternary Science Reviews*, 29, 1957–1959.
- Tejedor, E., de Luis, M., Cuadrat, J.M., Esper, J. and Saz, M.A. (2016) Tree-ring-based drought reconstruction in the Iberian range (east of Spain) since 1694. *International Journal of Biometeorology*, 60, 361–372.
- Toreti, A., Desiato, F., Fioravanti, G. and Perconti, W. (2009) Seasonal temperatures over Italy and their relationship with low-frequency atmospheric circulation patterns. *Climatic Change*, 99, 211–227.
- Touchan, R., Funkhouser, G., Hughes, M.K. and Erkan, N. (2005) Standardized precipitation index reconstructed from Turkish tree-ring widths. *Climatic Change*, 72, 339–353.
- Trouet, V., Panayotov, M.P., Ivanova, A. and Frank, D. (2012) A pan-European summer teleconnection mode recorded by a new temperature reconstruction from the northeastern Mediterranean (AD 1768–2008). *Holocene*, 22, 887–898.
- Trouet, V. and van Oldenborgh, G.J. (2013) KNMI climate explorer: a web-based research tool for high-resolution paleoclimatology. *Tree Ring Res.*, 69, 3–13.
- Trouet, V. (2014) A tree-ring based late summer temperature reconstruction (AD 1675–1980) for the Northeastern Mediterranean. *Radiocarbon*, 56, 69–78.
- Trouet, V., Babst, F. and Meko, M. (2018) Recent enhanced high-summer North Atlantic Jet variability emerges from three-century context. *Nature Communications*, 9, 180–189.
- Usoskin, I.G., Mursula, K. and Kovaltsov, G.A. (2002) Lost sunspot cycle in the beginning of Dalton minimum: New evidence and consequences. *Geophysical Research Letters*, 29, 2183. <https://doi.org/10.1029/2002GL015640>.
- Vicente-Serrano, S.M., Lopez-Moreno, J.I., Beguería, S., Lorenzo-Lacruz, J., Sanchez-Lorenzo, A., Garcia-Ruiz, J.M., Azorin-Molina, C., Morán-Tejeda, E., Revuelto, J., Trigo, R., Coelho, F. and Espejo, F. (2014) Evidence of increasing drought severity caused by temperature rise in southern Europe. *Environmental Research Letters*, 9, 044001. <https://doi.org/10.1088/1748-9326/9/4/044001>.
- Wigley, T., Briffa, K.R. and Jones, P.D. (1984) On the average of correlated time series, with applications in dendroclimatology and hydrometeorology. *Journal of Climate and Applied Meteorology*, 23, 201–213.
- Xoplaki, E., Gonzalez-Rouco, J.F., Gyalistras, D., Luterbacher, J., Rickli, R. and Wanner, H. (2003a) Interannual summer air temperature variability over Greece and its connection to the large-scale atmospheric circulation and Mediterranean SSTs 1950–1999. *Climate Dynamics*, 20, 537–554.

- Xoplaki, E., Luterbacher, J., Fidel González Rouco, J. and Wanner, H. (2003b) Mediterranean summer air temperature variability and its connection to the large-scale atmospheric circulation and SSTs. *Climate Dynamics*, 20, 723–739.
- Xoplaki, E., Gonzalez-Rouco, J.F., Luterbacher, J. and Wanner, H. (2004) Wet season Mediterranean precipitation variability: influence of large-scale dynamics and trends. *Climate Dynamics*, 23, 63–78.
- Xoplaki, E., Fleitmann, D., Luterbacher, J., Wagner, S., Haldon, J.F., Zorita, E., Telelis, I., Toreti, A. and Izdebski, A. (2016) The medieval climate anomaly and Byzantium: a review of the evidence on climatic fluctuations, economic performance and societal change. *Quaternary Science Reviews*, 136, 229–252.
- Zumbühl, H.J. and Nussbaumer, S.U. (2017) Little ice age glacier history of the central and Western Alps from pictorial documents. *Cuadernos de Investigación Geográfica*, 44, 115.

SUPPORTING INFORMATION

Additional supporting information may be found online in the Supporting Information section at the end of the article.

How to cite this article: Klippel L, Krusic PJ, Konter O, St. George S, Trouet V, Esper J. A 1200+ year reconstruction of temperature extremes for the northeastern Mediterranean region. *Int J Climatol*. 2018;1–15. <https://doi.org/10.1002/joc.5955>